Am J Cancer Res 2022;12(5):1960-1981
www.ajcr.us /ISSN:2156-6976/ajcr0134349

Original Article

MYBL2 accelerates epithelial-mesenchymal transition and hepatoblastoma metastasis via the Smad/SNAI1 pathway

Meng Wei[1], Ran Yang[1], Mujie Ye[1], Yong Zhan[1], Baihui Liu[1], Lingdu Meng[1], Lulu Xie[1], Min Du[1,2], Junfeng Wang[1], Runnan Gao[1], Deqian Chen[1], Rui Dong[1*], Kuiran Dong[1*]

[1]Department of Pediatric Surgery, Children's Hospital of Fudan University, 399 Wanyuan Road, Shanghai 201102, China; [2]Chengdu Women's and Children's Central Hospital, School of Medicine, University of Electronic Science and Technology of China, Chengdu 610091, China. [*]Equal contributors.

Received April 16, 2021; Accepted March 19, 2022; Epub May 15, 2022; Published May 30, 2022

Abstract: Hepatoblastoma (HB) accounts for the majority of hepatic malignancies in children. Although the prognosis of patients with HB has improved in past decades, metastasis is an indicator of poor overall survival. Herein, we applied single-cell RNA sequencing to explore the transcriptomic profiling of 25,264 metastatic cells isolated from the lungs of two patients with HB. The transcriptomes uncovered the heterogeneity of malignant cells after metastatic lung colonization, and these cells had varied expression signatures associated with the cell cycle, epithelial-mesenchymal plasticity, and hepatic differentiation. Single-cell regulatory network inference and clustering (SCENIC) was utilized to identify the co-expressed transcriptional factors which regulated and represented the different cell states. We further screened the key factor by bioinformatics analysis and found that MYBL2 upregulation was significantly associated with metastasis and poor prognosis. The relationship between ectopic MYBL2 and metastasis was subsequently proved by immunohistochemistry (IHC) of HB tissues, and the functions of MYBL2 in promoting proliferation, migration, and epithelial-to-mesenchymal transition (EMT) were verified by in vitro and in vivo assays. Importantly, the levels of Smad2/3 phosphorylation and SNAI1 expression were increased in *MYBL2*-transfected cells. Consequently, these results indicated that the MYBL2-controlled Smad/SNAI1 pathway induced EMT and promoted HB tumorigenesis and metastasis.

Keywords: Epithelial-to-mesenchymal transition, hepatoblastoma, metastasis, MYBL2, single-cell RNA sequencing, SNAI1

Introduction

As the most common hepatic malignancy in infants and young children, hepatoblastoma (HB) accounts for approximately 1% of all pediatric tumors [1, 2]. Although combined therapies have improved the prognosis of HB, metastasis is still a predictor of poor overall survival, with approximately one-fifth of patients progressing to de novo metastatic HB [3, 4]. The 5-year overall survival rate of patients with pulmonary metastasis due to HB is about 21-28%, and the progression-free survival rate is only 21-28% [5-7]. Currently, chemotherapy and resection are the combined treatment methods for lung metastasis, with less than 50% of patients achieving complete remission after chemotherapy [5, 8]. Patients with HB whose tumors remained unresectable after chemotherapy can choose liver transplantation, but unresectable lung metastasis will rule out the possibility of liver transplantation and greatly affect the survival of patients. Therefore, the molecular mechanism and clinical treatment of patients with pulmonary metastasis due to HB remain difficult challenges that require additional efforts, and the prognosis of these patients needs to be further improved.

Epithelial-to-mesenchymal transition (EMT) is postulated to trigger metastatic progression, which is followed by intravasation, dissemination, extravasation, and micro-metastases to palpable macro-metastases [9]. Cancer cells lose epithelial features and gain mesenchymal phenotypes, and this process is mediated by

EMT-driving transcription factors (TFs), primarily the members of SNAIL, TWIST, and ZEB families. Albeit its metastasis-initiating function is controversial, EMT has been considered to regulate physiological growth and development, as well as drug resistance [10-12].

The MYB transcription factor family consists of three members: MYB (C-MYB), MYBL1 (A-MYB), and MYBL2 (B-MYB). MYB expression is limited to hematopoietic cells, colonic crypts, and the brain. MYBL1 is mainly expressed in B lymphocytes, germ cells of the brain, and germinal centers of the spleen, while MYBL2 is widely expressed in proliferating cells. Consistent with the unique distribution of MYB family members, the abnormal expression of MYB is associated with the occurrence of tumors of the blood, colon, and breast, as well as other malignant tumors [13]. Ectopic MYBL1 expression is associated with hematological tumors [14], while MYBL2 expression may be closely correlated with the occurrence and development of malignant tumors from various tissues and organs. Studies have found that MYBL2 plays a role in a variety of tumors, such as renal clear cell carcinoma [15], prostate cancer [16], non-small cell lung cancer [17-19], liver cancer [20], and gastric cancer [21]. The level of MYBL2 expression in various tumors is significantly higher than that in adjacent tissues, which promotes tumor cell proliferation, drug resistance, and distant metastasis, and thus, is associated with the poor prognosis of patients [22, 23].

The level of MYBL2 expression, as well as the role of MYBL2, in HB progression has not been investigated yet. In this study, we performed single-cell RNA sequencing (scRNA-seq) on pulmonary metastatic tumor tissues to investigate the transcriptional profile, heterogeneity, and cellular plasticity of tumor cells. Bioinformatics analysis indicated that MYBL2 may be a predictor of metastasis and poor survival of patients with HB. The results of mechanistic studies showed that increased MYBL2 expression promoted EMT by activating the Smad signaling pathway. Furthermore, the level of SNAI1 expression was upregulated as the MYBL2-induced Smad pathway was activated. Both EMT and SNAI1 expression were reversed in MYBL2-overexpressing cells, which were cultured in the presence of the Smad pathway inhibitor. These results implied that MYBL2 promoted EMT, tumor migration, and metastasis by activating the Smad/SNAI1 pathway.

Materials and methods

HB samples and cell lines

For scRNA-seq analysis, pulmonary metastatic tumor tissues of two patients with HB were acquired from the Children's Hospital of Fudan University (Shanghai, China). For RNA and protein extraction, freshly frozen specimens of hepatic tumors and adjacent noncancerous hepatic tissues from 24 patients, who underwent hepatectomy for HB between 2020 and 2021, were obtained from the Children's Hospital of Fudan University. For immunohistochemistry (IHC), paraffin-embedded sections of tumor tissues from 78 patients with HB were collected between 2011 and 2019 from the Children's Hospital of Fudan University. All samples were collected after obtaining written informed consent from the guardian(s) of each patient, and the study was approved by the ethical committee of this hospital. HB cell lines (HuH6 and HepG2) were purchased from the Chinese Academy of Medical Sciences (Shanghai, China).

Preparation of single-cell suspensions

Pulmonary metastatic tumor samples were collected during surgery. The samples were shredded mechanically and enzymatically digested with collagenase IV and DNase I for 30 min at 37°C with agitation. Thereafter, we sieved the suspension through a 70 μm cell strainer, washed the filtered cells with 1% BSA and 2 mM EDTA in PBS, and centrifuged the resulting suspension for 8 min at 500× *g*. Single-cell suspensions were run through Lympholyte-H separation medium to remove red blood cells and debris according to the manufacturer's specifications.

Droplet-based scRNA-seq data pre-processing and quality control (QC)

Droplet-based scRNA-seq analyzes single cells using the GemCode platform and the Chip and Library kit (10× Genomics), which constructs the scRNA-seq library [24]. Using the Chromium Controller system, cell suspensions from each metastatic tumor sample were prepared

with appropriate reagents to generate single-cell gel bead-in-emulsions (GEMs) and barcoded. Libraries were then sequenced on the NovaSeq 6000 system (Illumina) with a depth of approximately 400 M reads.

FASTQ files of raw sequencing data were generated with Illumina bcl2fastq software (version 2.19.1) and mapped to the GRCH38 human genome reference using the Cell Ranger toolkit (version 2.1.1), in which the digital gene-cell expression matrix was processed from the data by demultiplexing, barcode processing, and single-cell 3' gene counting. Seurat package (version 2.3.4) was applied to prune low-quality cells in this gene-cell expression matrix, which contained <500 genes and >10% mitochondrial genes [25].

Single-cell RNA-seq data downstream analysis

To identify cell subsets for each sample dataset, Seurat's Normalize Data function was applied to normalize and log-transform the filtered gene-cell expression matrix [26]. Thereafter, principal component analysis (PCA) was used to reduce dimensionality with highly variable genes. We merged the two samples by applying Harmony integration, which retained biological differences but eliminated technological batches [27]. Graph-based clustering, *t*-distributed stochastic neighbor embedding (t-SNE), and uniform manifold approximation and projection (UMAP) were employed for clustering and visualization.

Large-scale chromosomal copy-number variations (CNVs) were identified in malignant cells by sequencing genes based on their chromosomal orientation and employing a moving average of the relative expression values [28, 29]. Endothelial cells were taken as the "normal" reference and then subtracted from all cells. The hidden Markov model (HMM) was applied to calculate the CNV level, and we focused on chromosomes with 1q gain, 2q gain, and 1p loss in each cell, which agreed with the genetic hallmarks of HB derived from bulk sample sequencing [30].

Non-negative matrix factorization (NMF) was used to refine the transcriptional programs of malignant cells isolated from each tumor (with the number of factors set to 10). Each factor was characterized by the top 50 genes. Four correlated sets of meta-programs were extracted using Pearson correlation coefficients and Ward's linkage.

The Python package, "pySCENIC", was applied for SCENIC analysis. Given the predefined TF list, the primary regulatory network was inferred by GRNBoost (SCENIC version 0.1.5) from the processed matrix. TF-target interactions in single cells were further filtered by following the cisTarget step. Databases were downloaded from https://resources.aertslab.org/cistarget/.

Using the velocity pipeline, we generated loom files to annotate spliced and unspliced reads. Thereafter, loom files were loaded in R to produce count matrices for spliced/unspliced reads, followed by analysis with the scVelo Python package [31].

We estimated the prognostic prediction of *MYBL2* using the patient's dataset (n=53) downloaded from the Gene Expression Omnibus database (GEO: GSE131329).

Western blotting

Anti-MYBL2 (Abcam-12296, 1:2500), anti-ZO-1 (Invitrogen-33-9100, 1:1000), anti-GAPDH (Proteintech-60004, 1:5000), anti-FN1 (Cell Signaling-26836, 1:1000), anti-AKT (Cell Signaling-9272, 1:1000), anti-phospho-Akt (Ser-473) (Cell Signaling-4060, 1:2000), anti-GSK-3β (Cell Signaling-9832, 1:1000), anti-phospho-GSK-3β (Ser9) (Cell Signaling-9323, 1:1000), anti-Smad2/3 (Cell Signaling-8685, 1:1000), anti-phospho-Smad2/3 (Cell Signaling-8828, 1:1000), anti-ERK1/2 (Cell Signaling-9102, 1:1000), anti-phospho-ERK1/2 (Cell Signaling-4370, 1:2000), and anti-SNAI1 (Abcam-216347, 1:1000) primary antibodies were used. HRP-linked anti-IgG (Cell Signaling, 1:5000) was used as the secondary antibody.

Quantitative real-time PCR (QPCR)

The RNAiso Plus kit (TaKaRa) was used to extract total RNA from HB cell lines and tissues. Genes of interest were tested using SYBR® Premix Ex Taq (TaKaRa). The primer sequences are listed in Table S1.

Construction of stably transfected cells

Lentiviral vectors encoding MYBL2 and MYBL2 shRNAs were purchased from Genomeditech (Shanghai, China), and 293T cells were used

for lentivirus packaging. HepG2 and HuH6 cells were individually infected with the produced viruses. The levels of MYBL2 overexpression and knockdown were examined by QPCR and western blotting.

Cell proliferation assay

The Cell Counting Kit-8 (CCK-8) and EdU kit (Beyotime, Shanghai, China) were used to examine the proliferation of HB cells. For the CCK-8 assay, cells were seeded in 96-well cell culture plates at a density of 6,000 cells per well, and the absorbance of each well was measured at 450 nm after incubation with 10% CCK-8 reagent for 2.5 h. For the EdU assay, cells were stained after incubation with 50 μM EdU for 2 h.

Cell migration assay

For the cell migration assay, 1×10^5 cells were seeded into the upper chambers of 12-μm micropore inserts (Millipore, America) in medium without FBS, and medium with 20% FBS was added into the lower chambers of the micropore inserts. Forty-eight hours later, migratory cells under the inserts were fixed and stained with 0.25% crystal violet for 45 min.

Immunohistochemistry

Tumor and adjacent non-tumor samples were fixed in formalin, embedded in paraffin, de-paraffinized, and rehydrated. To retrieve antigens, sections were treated with 10 mM sodium citrate (pH 6) at 100°C for 10 min. Thereafter, non-specific antibody binding sites were blocked with 5% BSA for 1 h at room temperature. Sections were incubated with primary antibodies overnight at 4°C in blocking buffer. On the following day, sections were washed three times in PBS (5 min each time), followed by incubation with secondary antibodies (GeneTech, 1:500) for 1 h at room temperature. The primary antibodies were anti-MYBL2 (Cell Signaling-191064, 1:500) and anti-Ki67 (Abcam-16667, 1:200). The level of MYBL2 expression was evaluated by scoring the staining intensities according to the staining index (SI) [32].

In vivo tumorigenicity assays

Five-week-old male nude mice were obtained from Gempharmatech (Jiangsu, China). For assessing cell proliferation in vivo, 5×10^6 cells were suspended in 100 μL of medium without FBS, which contained 50% Matrigel (Corning, NY, USA), and subcutaneously implanted under the right armpits of mice (n=8/group). We observed and measured the tumor size every 4 days. The formula for calculating tumor volume was as follows: $V=0.5\times (\text{length}) \times (\text{width})^2$.

Statistical analysis

Statistical analysis was performed using R (version 3.4.3) and GraphPad Prism (version 7.04). A p-value <0.05 was considered statistically significant. Details of statistical tests are provided in results and figure legends.

Results

Single-cell transcriptome profiling of HB metastases

To investigate the molecular mechanism of metastasis in patients with HB, we performed scRNA-seq for two pulmonary metastatic lesions collected during surgical resection using a 10× genomic platform (**Figure 1A-C**). After initial quality controls, we retained and distinguished 19,058 malignant cells and 6,206 non-malignant cells based on the expression of epithelial markers and the composition of karyotypes. We recognized malignant cells by their epithelial characteristics, namely, the expression of EPCAM, KRT8, and KRT18 (**Figure 1D**, **1E**). Pulmonary epithelial cells were further identified according to their distinctive expression of FOXJ1 and SFTPC. Thereafter, the remaining epithelial cells were confirmed as malignant by identifying large-scale CNVs based on the transcriptome of each single cell [29, 33, 34]. These supposedly malignant cells from both metastatic lesions showed concordantly segmental chromosome 1q gain, 2q gain, and 1p loss, as previously described for HB [30, 35]. In addition, a gain in chromosome 6 was observed in myeloid cells, which may have been caused by human leukocyte antigen genes on chromosome 6 (**Figure 2E**, **2F**) [36]. Consistent with our results on malignant cells, which were identified by differences in epithelial marker expression, these cells were further confirmed by comparing collectively aberrant karyotypes with the negative results of non-malignant cells.

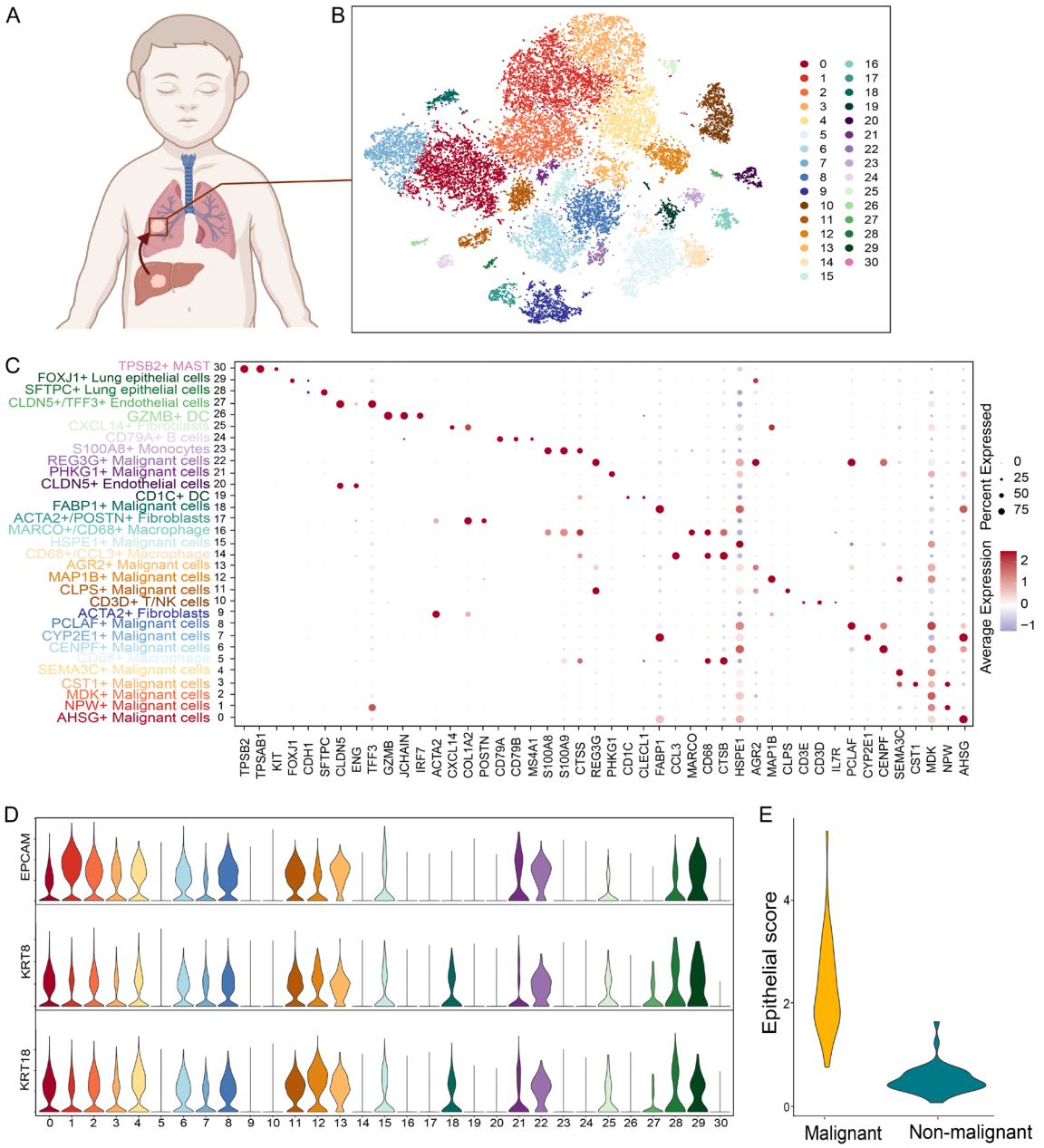

Figure 1. Single-cell transcriptome profiling of HB metastases. A. Tissue origin collected in this study. Transcriptional profiling of lung metastatic cells was analyzed by scRNA-seq. B. tSNE plot of all 25,264 cells from two metastatic samples with 31 clusters. C. Dot plot of mean expression of recognized or cell-type-specific markers for all clusters. D. Violin plot of epithelial marker genes (average expression of *EPCAM*, *KRT8*, *KRT18*) for all clusters. E. Besides lung epithelial cells, whole cells from two metastatic samples were classified as tentatively malignant or non-malignant according to the expression of classical markers and the divergency in epithelial or mesenchymal origin. The epithelial scores of malignant cells were significantly higher than those of stomal and immune cells.

Non-malignant cells were classified according to acknowledged marker expression and manually annotated into six major lineages, namely, B cells (CD79A and CD79B); myeloid cells, including macrophages (CD68 and MARCO), monocytes (S100A8 and S100A9), DC (CD1C and GZMB), MAST (TPSB2 and TPSAB1); T cells (CD3D and CD3E); fibroblasts (ACTA2 and COL1A2); endothelial cells (CLDN5 and KDR); and lung epithelial cells (FOXJ1 and SFTPC) (**Figure 2A-D**). Heterogeneity was observed among immune, stromal, and malignant cells

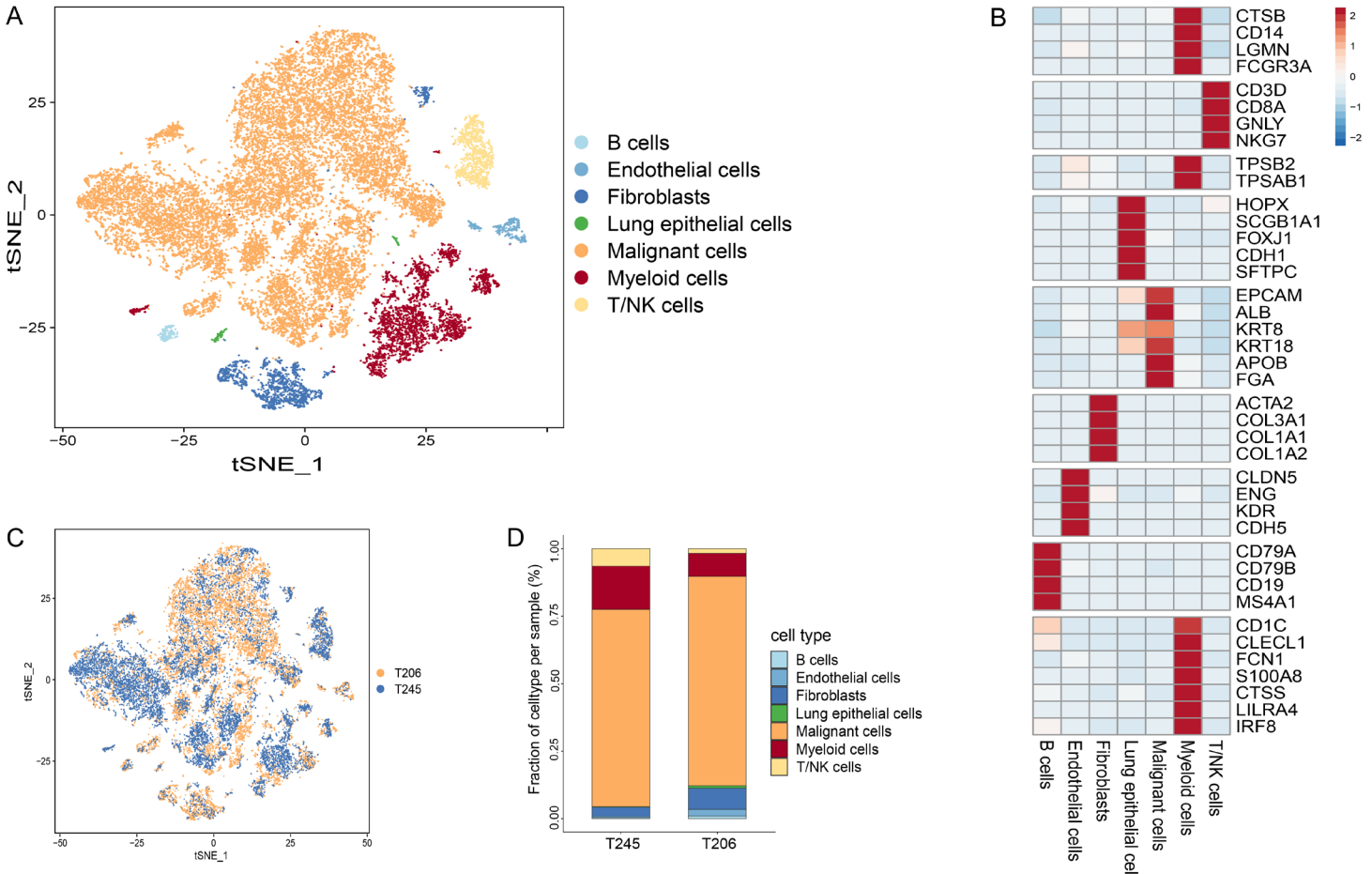
A
tSNE_2
tSNE_1
B cells
Endothelial cells
Fibroblasts
Lung epithelial cells
Malignant cells
Myeloid cells
T/NK cells
B
CTSB
CD14
LGMN
FCGR3A
CD3D
CD8A
GNLY
NKG7
TPSB2
TPSAB1
HOPX
SCGB1A1
FOXJ1
CDH1
SFTPC
EPCAM
ALB
KRT8
KRT18
APOB
FGA
ACTA2
COL3A1
COL1A1
COL1A2
CLDN5
ENG
KDR
CDH5
CD79A
CD79B
CD19
MS4A1
CD1C
CLECL1
FCN1
S100A8
CTSS
LILRA4
IRF8
C
T206
T245
D
Fraction of celltype per sample (%)
cell type
T245
T206

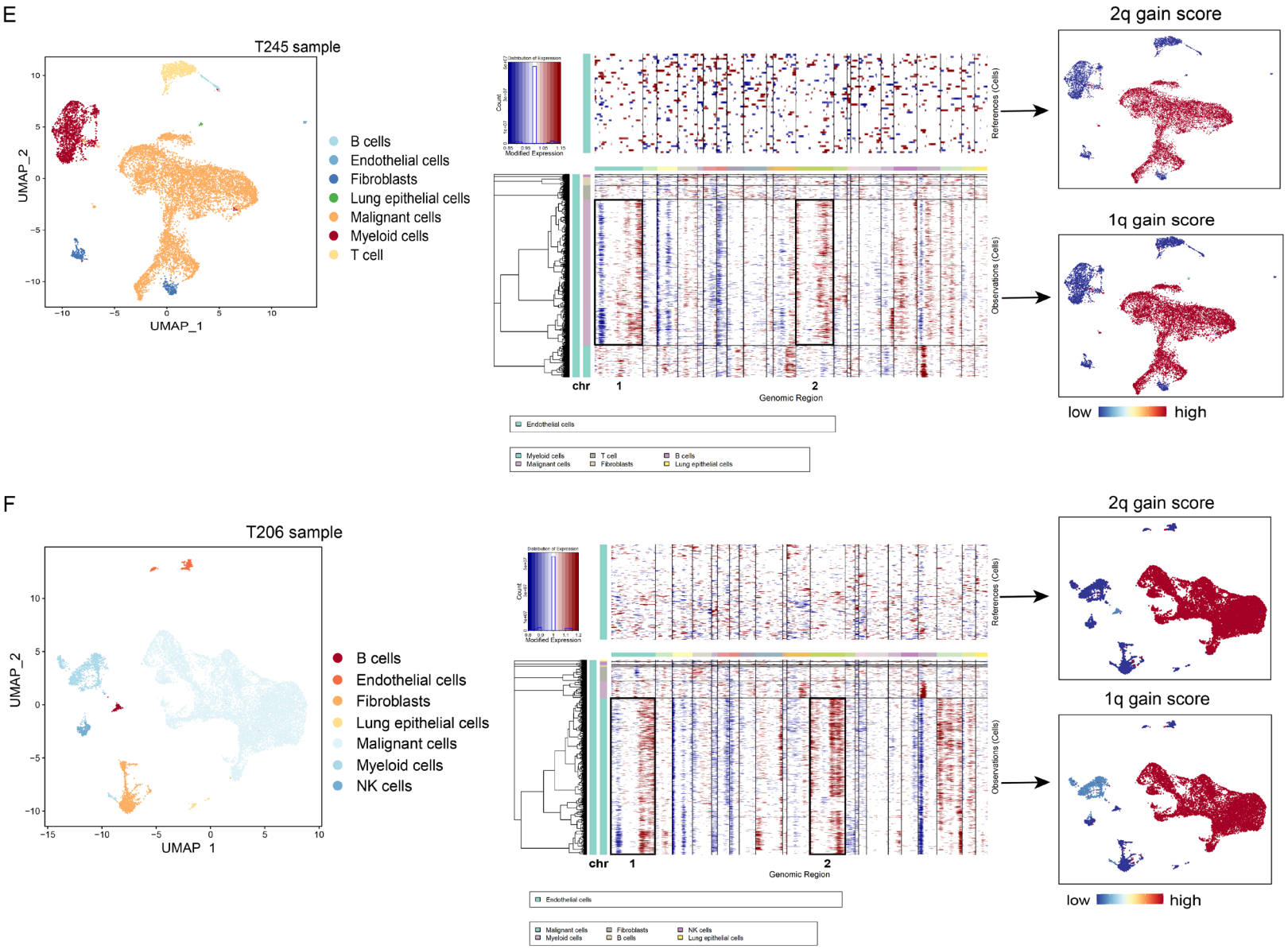

Figure 2. Composition and differentially expressed genes of seven cell lineages from two metastatic tumors. A. Based on the two-step method to identify malignant cells, 25,264 cells from two metastatic samples (T245 and T206) were classified into seven cell lineages. B. Heatmap of characteristic marker genes expressed in all cell types from T245 and T206 samples. Mean-centering, which was used to scale the values of mean expression, ranged from -2 to 2. C. Colored UMAP of the

respective sample origin. D. Bar graph of cell type fractions in each sample. E. Top: UMAP visualization of seven cell types from the T245 sample; bottom-left: heatmap of large-scale CNVs from all cells; bottom-right: UMAP visualization of the distribution of the copy number gain of chromosomes 1q and 2q. F. Top: UMAP visualization of seven cell types from the T206 sample; bottom-left: heatmap of large-scale CNVs from all cells; bottom-right: UMAP visualization of the distribution of the copy number gain of chromosomes 1q and 2q.

isolated from both metastatic lesions. Both T cells (cl. 10) and B cells (cl. 24) had one cell cluster, endothelial cells (cl. 20, 27) and lung epithelial cells (cl. 28, 29) had two, fibroblasts (cl. 9, 17, 25) contained three, myeloid cells (cl. 5, 14, 16, 19, 23, 26, 30) had seven, and malignant cells were separated into 15 clusters (**Figure 1C**). Furthermore, cells of different origins (T206 and T245) were collectively involved in the make-up of each cluster without one patient-specific subpopulation, demonstrating agreement between cell type diversity and expression profiles between the two metastatic lesions (**Figure 2C**).

Intra-tumoral heterogeneity of pulmonary metastatic cells

Following the identification of the different cell types in both metastatic lesions, we explored the transcriptional characteristics of these malignant cells. The NMF algorithm was applied to analyze transcriptional signatures that were co-expressed by versatile subpopulations of malignant cells [37]. Twenty verified signatures were partitioned into four major meta-programs, namely, three irrelevant meta-programs (A, B, and D) and one unspecific program (C) (**Figures 3A-E**, **4A**, **4B**, **4D**).

The three meta-programs (A, B and D) were characterized by heterologous functions that were revealed by high-scoring genes (**Figure 3D**). Genes in meta-program A were related to EMT plasticity (e.g., EPCAM, VIM, SOX4, and ID1 expression) in which mesenchymal features were co-expressed with epithelial markers, demonstrating the hybrid state of the dynamic process. The dual functions of ID1 in promoting metastasis have been previously reported. ID1 can contribute to the increased motility of primary tumor cells by triggering EMT, which subsequentially drives the colonization of cells to a remote organ by altering the cellular state from EMT to mesenchymal-to-epithelial transition (MET) [38]. The possibility of cell doublets was excluded by the identification of doublets in this population (**Figure 3H**). The top-scoring markers of the meta-program B indicated a differentiated state of the hepatocyte-like phenotype (e.g., FGB and AFP expression), whereas those of the meta-program D were mainly involved in the cell-cycle (e.g., TOP2A, MKI67, and CDK1 expression). These findings supported the transcriptional heterogeneity underlying the different cellular states.

After deciphering the transcriptional spectrum underlying the malignant cells of the secondary tumors, we applied the RNA velocity approach to trace the fate of the metastatic cells and analyze the dynamics of intratumorally cellular states. Both T206 and T245 metastatic tumors exhibited EMT, as shown by the predicted fate of epithelial cells with increased expression of VIM and decreased CDH1 expression (**Figures 3F**, **3G** and **4C**). The existence of EMT in secondary tumors may have promoted and maintained the aggressive properties of metastatic cells.

Transcriptional heterogeneity controlled by TFs regulator networks

To identify the regulatory factors underlying the malignant cell states with heterogeneously transcriptional spectrums, SCENIC analysis was applied for malignant cells isolated from both metastatic lesions [39]. We identified specific co-expressed TFs and their potential targets, which were related to the three meta-programs uncovered by NMF analysis (**Figure 5A**, **5B**). Enriched regulators of the meta-program A included TRPS1, TWIST2, ELF1, HIVEP2, SOX4, and IRX2, and these genes were linked to the switching of epithelial and mesenchymal cell states. Except for TWIST2, other EMT regulators-namely, ZEB1/2, TWIST1, and SNAIL1/2-were undetected in malignant cells. TRPS1 has been reported to participate in the suppression of cell motility and EMT in malignant cells, as well as in the regulation of MET during embryonic development [40, 41]. TWIST2 can induce the EMT phenotype and liver stem cell-like self-renewal by regulating CD24 [42]. In addition, ELF1 played a critical role in tumor cell plasticity by contributing to heterogeneous pheno-

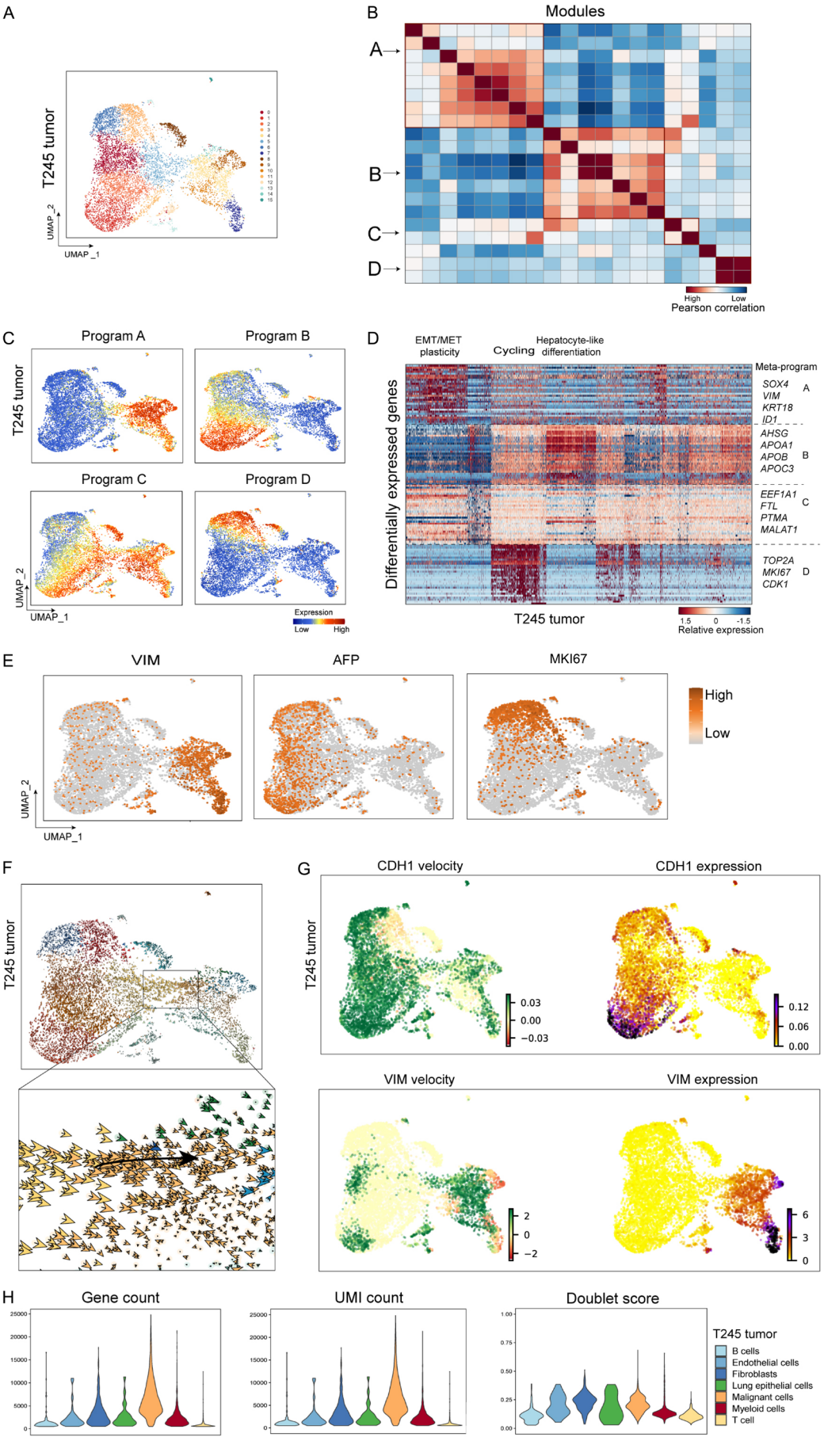
A
T245 tumor
UMAP_2
UMAP_1
B
Modules
A
B
C
D
High
Low
Pearson correlation
C
Program A
Program B
Program C
Program D
T245 tumor
UMAP_2
UMAP_1
Expression
Low
High
D
EMT/MET plasticity
Cycling
Hepatocyte-like differentiation
Meta-program
SOX4
VIM
KRT18
ID1
A
AHSG
APOA1
APOB
APOC3
B
EEF1A1
FTL
PTMA
MALAT1
C
TOP2A
MKI67
CDK1
D
Differentially expressed genes
T245 tumor
1.5
0
-1.5
Relative expression
E
VIM
AFP
MKI67
High
Low
UMAP_2
UMAP_1
F
T245 tumor
G
CDH1 velocity
CDH1 expression
T245 tumor
0.03
0.00
−0.03
0.12
0.06
0.00
VIM velocity
VIM expression
2
0
−2
6
3
0
H
Gene count
UMI count
Doublet score
T245 tumor
B cells
Endothelial cells
Fibroblasts
Lung epithelial cells
Malignant cells
Myeloid cells
T cell

Figure 3. EMT course identified by NMF and RNA velocity analysis of malignant cells from the T245 sample. (A) Feature plot of malignant cells from the T245 sample with 16 clusters. (B) Heatmap depicts the correlation of 20 programs extracted by NMF analysis for two samples (T245 and T206). Four correlated meta-programs (A-D) are recognized and highlighted. (C) Feature plot of gene sets of four meta-programs specifically expressed in malignant cells of the T245 tumor. (D) Heatmap of four meta-programs of malignant cells (T245 tumor) identified by NMF analysis and grouped according to differentially expressed genes (rows). (E) Feature plot of VIM, AFP, and MKI67 expression in malignant cells from the T245 tumor. (F) RNA velocity vector field at the single-cell level, manifested as arrows, delineates the direction and speed of each malignant cell from the T206 tumor. (G) RNA velocity and expression of CDH1 and VIM. (H) Quality control coefficients for whole cells clustered by cell type (T245 sample).

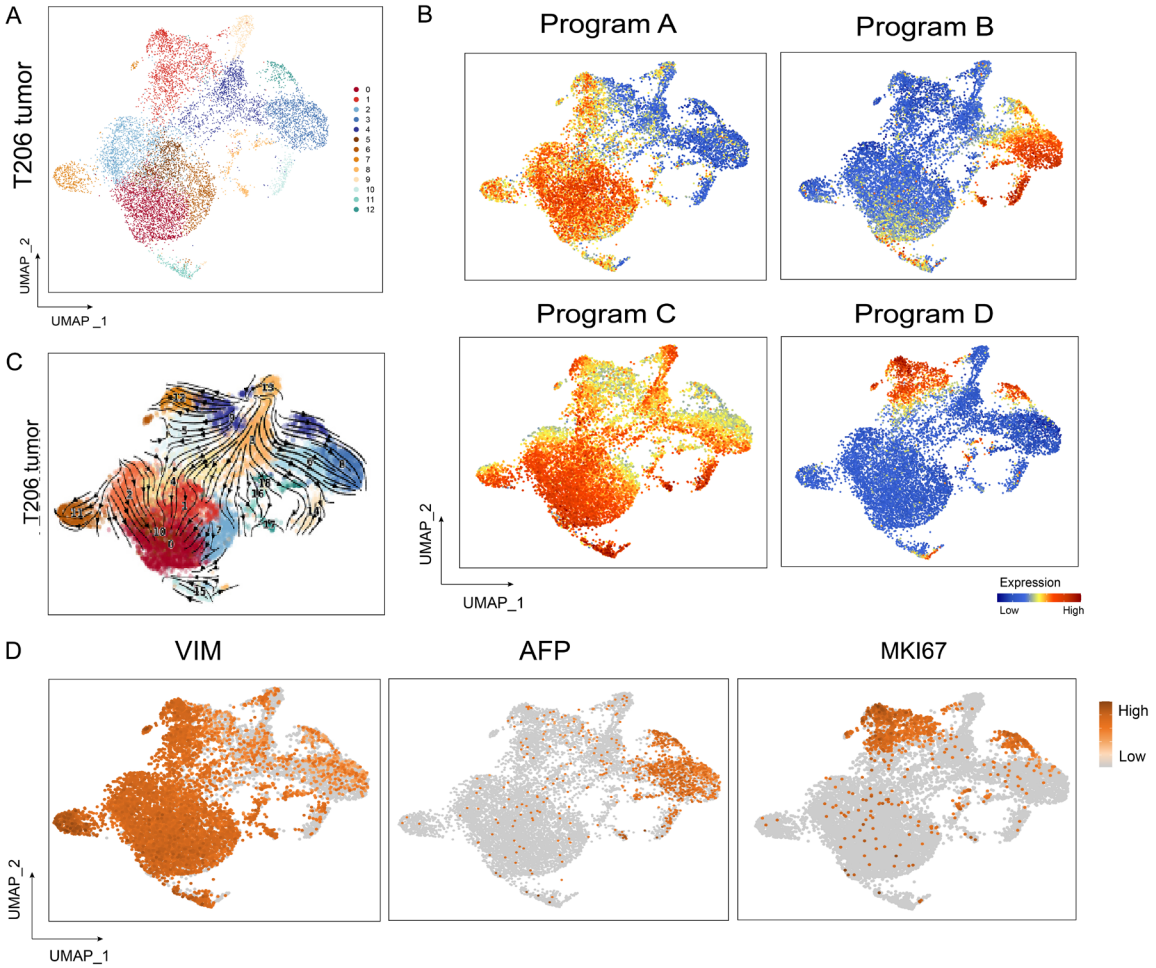

Figure 4. EMT course identified by NMF and RNA velocity analysis of malignant cells from the T206 sample. A. Feature plot of malignant cells from the T206 sample with 13 clusters. B. Feature plot of gene sets of four meta-programs specifically expressed in malignant cells from the T206 tumor. C. RNA velocity vector field, manifested as streamlines, delineates the future states of malignant cells from the T206 tumor. D. Feature plot of VIM, AFP, and MKI67 expression in malignant cells from the T206 tumor.

types and cellular states. Wouters et al. reported that the intermediate state of melanoma, an invasive or dedifferentiated phenotype, was regulated by active regulators such as ELF1, SOX6, and EGR3 [43-46].

The top-scoring regulons of the meta-program B were RORC, HLF, PPARG, EPAS1, and NFATC2. PPARG and EPAS1 have been reported to induce cell differentiation or enhance chemosensitivity [47-49]. However, the associations between the increased expression of RORC, HLF and NFATC2 and the increased risk of metastasis have not been reported yet. We next identified FOXA1, ZNF281, BRCA1, MYBL2, and POLE3 as dominating regulators of the meta-

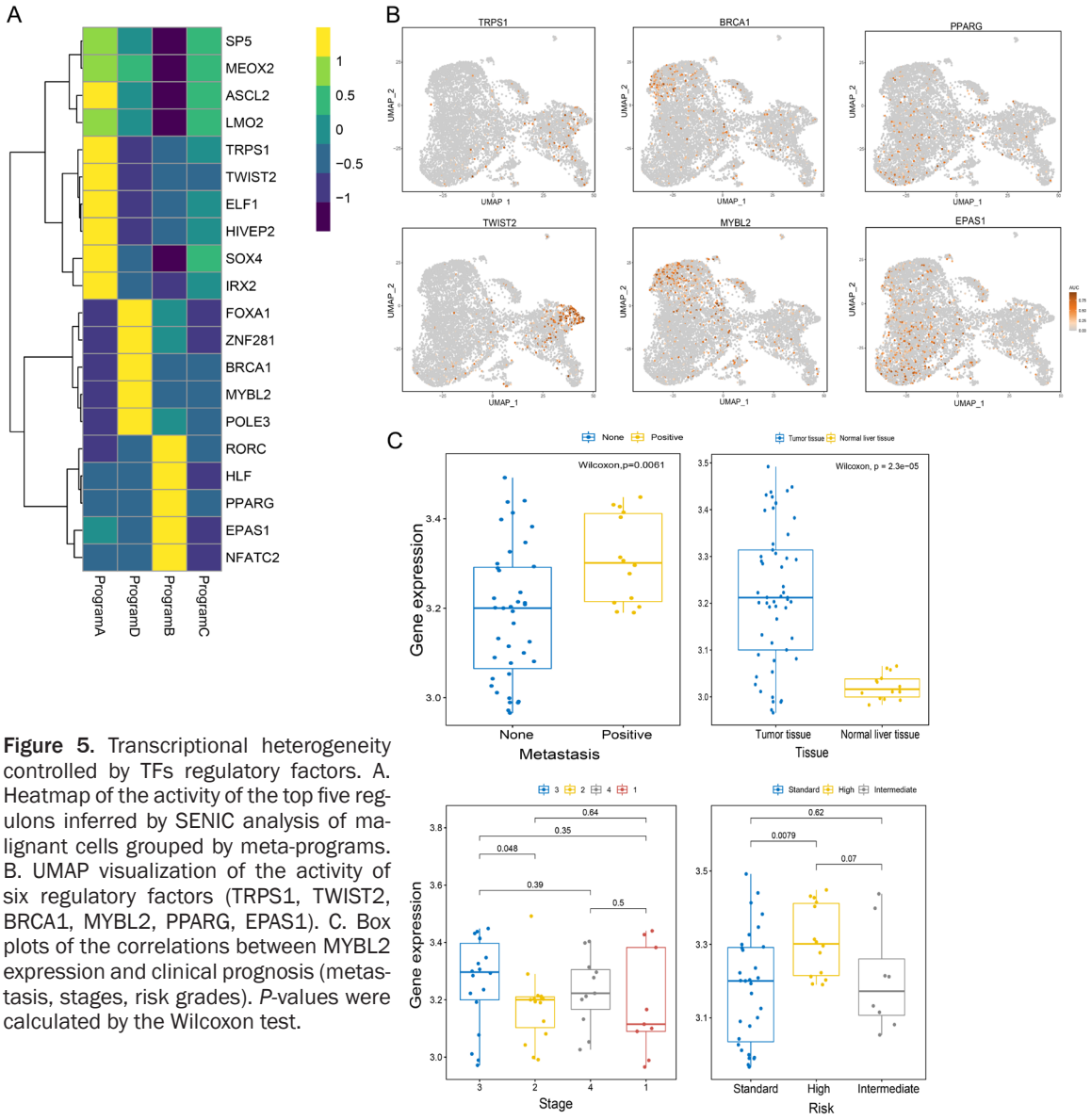

Figure 5. Transcriptional heterogeneity controlled by TFs regulatory factors. A. Heatmap of the activity of the top five regulons inferred by SENIC analysis of malignant cells grouped by meta-programs. B. UMAP visualization of the activity of six regulatory factors (TRPS1, TWIST2, BRCA1, MYBL2, PPARG, EPAS1). C. Box plots of the correlations between MYBL2 expression and clinical prognosis (metastasis, stages, risk grades). *P*-values were calculated by the Wilcoxon test.

program D. Except for POLE3, these regulons could either suppress differentiation or increase proliferation [50-53]. The characteristics of gene regulator networks further verified the properties of meta-programs annotated by NMF analysis.

MYBL2 functions as an oncogene in HB and predicts metastasis and poor prognosis

To identify the key factor critical in manipulating the aggressiveness of HB and in predicting the poor prognosis of patients, we used microarray data from the GEO database (GSE1313-29) to screen the above regulators dominating the aggressiveness and metastasis of HB. The results indicated that MYBL2 expression was significantly higher in tumor tissues than that in normal tissues (P<0.0001), and MYBL2 overexpression was a prognostic factor of poor survival for patients with HB. Higher MYBL2 expression was correlated with the high-risk group (P<0.01), increased probability of metastasis (P<0.01), and higher stage (P=0.048) (**Figure 5C**).

Next, 48 freshly frozen HB tumor and matched para-tumor specimens were used to explore the discrepant expression of MYBL2. Compared with matched normal tissues, MYBL2 was overexpressed in tumor specimens (**Figure 6A-C**). Furthermore, paraffin-embedded tumor

specimens of 78 patients with HB were utilized to analyze the correlation of MYBL2 expression with clinical characteristics and prognosis (**Table 1**). Consistent with the biostatistical results derived from the GEO database, the expression levels of MYBL2 in tumor specimens of patients with distant lung metastasis (n=12) were higher than that without distant lung metastasis (n=66, P<0.01, **Figure 6D**). Furthermore, higher MYBL2 expression was associated with tumor thrombus (P<0.01), shorter overall survival (P=0.046), and shorter progression-free survival (P=0.0415, **Figure 6E-G**). Taken together, MYBL2 expression in patients with HB was associated with aggressive characteristics and served as a predictor of metastasis and poor survival.

MYBL2 enhances the proliferation and migration of HB cells in vitro

MYBL2 expression was higher in the HB cell line HuH6 than that in the HB cell line HepG2 and the normal hepatocyte cell line L02 (**Figure 7A**). Stable MYBL2-knockdown (HuH6) and MYBL2-overexpression (HepG2) cell lines were constructed to examine the biological activity of MYBL2 (**Figure 7B**). The results of CCK-8 and EdU assays showed that increased MYBL2 expression strongly promoted HB cell growth compared with that of controls. By contrast, reduced MYBL2 expression significantly weakened HuH6 cell proliferation (**Figure 7C**, **7D**). Taken collectively, these findings suggested that MYBL2 improved the growth of HB cells in vitro. Moreover, a transwell migration assay was conducted to assess the metastatic ability of HB cells. MYBL2 overexpression enhanced the migratory ability of HB cells, whereas reduced MYBL2 expression inhibited the migratory ability compared with that of controls (**Figure 7E**). These results demonstrated that elevated MYBL2 expression participated in HB progression.

MYBL2 accelerates HB cell growth in vivo

To verify the in vivo significance of aberrant MYBL2 expression in tumor cell growth, transfected cells were inoculated subcutaneously under the right armpit of nude mice. The elevated MYBL2 expression significantly accelerated the in vivo proliferation of the implanted cells compared with that of controls (**Figure 8A**). Furthermore, the levels of MYBL2 and Ki67 expression in subcutaneous tumors derived from *MYBL2*-transfected HepG2 cells, which were examined by IHC, were higher than those of controls (**Figure 8B**). By contrast, MYBL2 knockdown weakened tumor growth in vivo. Lower MYBL2 and Ki67 expression was observed in subcutaneous tumors derived from sh*MYBL2*-transfected HuH6 cells compared with tumors derived from control cells (**Figure 8C**, **8D**).

MYBL2 induces cell migration and metastasis by promoting SNAI1-independent Smad pathway-mediated EMT

The bioinformatics analysis of pulmonary metastatic tumor specimens from patients with HB proposed that various cellular states contributed to intratumor heterogeneity, including EMT, cell proliferation, and differentiation. EMT has been reported to participate in lung metastasis and tumorigenesis [54]. Therefore, we questioned the relationship between MYBL2 expression and EMT progression. EMT-associated proteins and EMT-related pathways were analyzed by western blotting using *MYBL2*-transfected and *MYBL2*-silenced cells. The epithelial marker ZO-1 was downregulated and the mesenchymal marker FN1 was upregulated in MYBL2-overexpressing cells. By contrast, reduced MYBL2 expression caused an upregulation of the ZO-1 level and a downregulation of the FN1 level (**Figure 9A**). These results demonstrated the ability of MYBL2 to regulate EMT.

To examine the participating signaling pathway in MYBL2-regulated EMT, changes in three EMT-relevant pathways, PI3K/AKT, Smad, and MAPK/ERK [55], were examined in *MYBL2*-transfected and sh*MYBL2*-transfected cells. Interestingly, in MYBL2-upregulated HepG2 cells, the phosphorylation level of Smad2/3 was significantly increased, whereas the phosphorylation level of Smad2/3 was decreased in MYBL2-downregulated HuH6 cells. Despite the findings that the levels of AKT phosphorylation and GSK-3β expression were increased in MYBL2-overexpressing cells, they showed no changes when MYBL2 expression was depleted. Furthermore, the level of ERK1/2 phosphorylation was increased as MYBL2 expression was reduced, and it showed no changes in MYBL2-overexpressing cells (**Figure 9B**). Taken

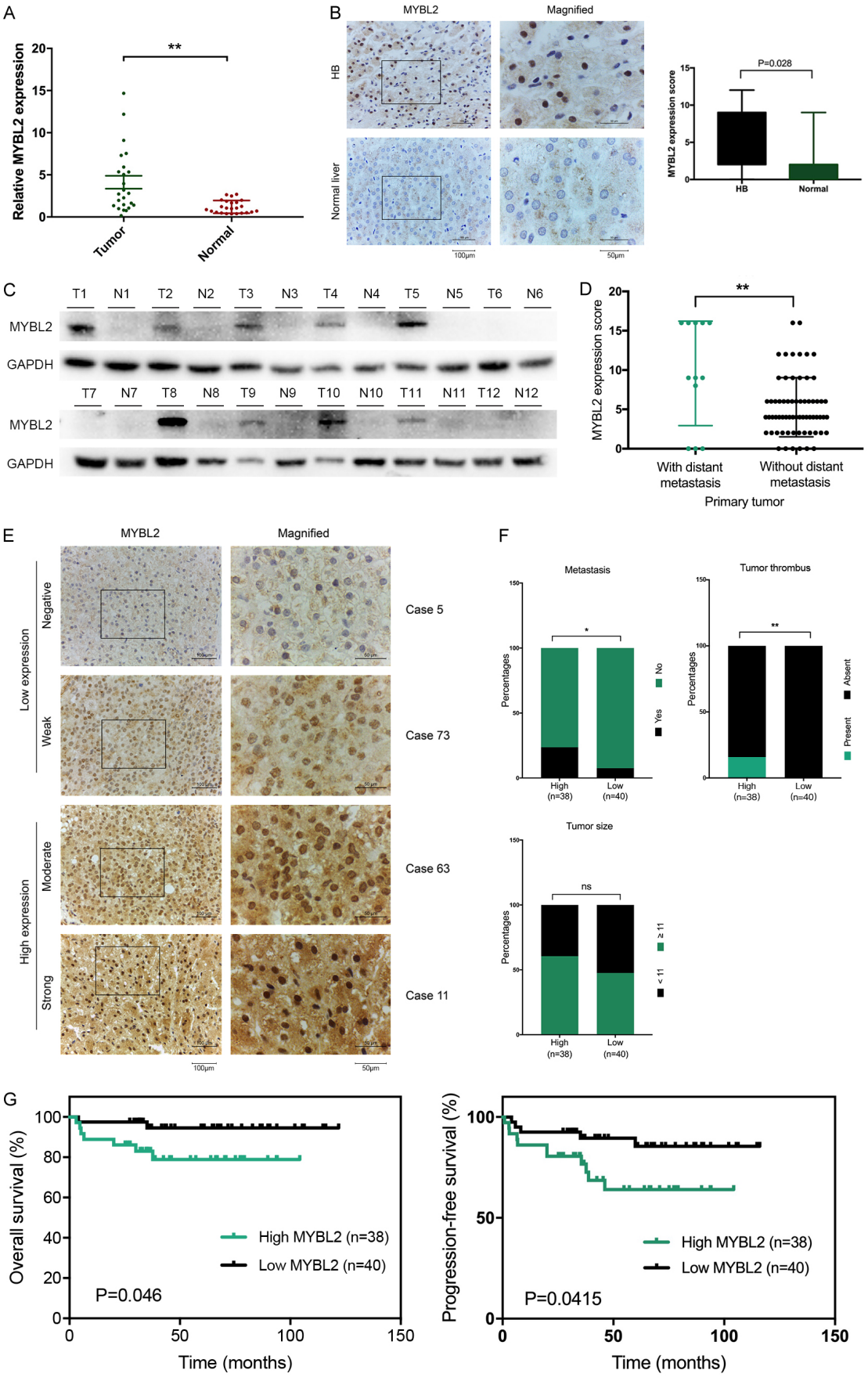
A
Relative MYBL2 expression
**
Tumor
Normal
B
MYBL2
Magnified
HB
Normal liver
100μm
50μm
P=0.028
MYBL2 expression score
HB
Normal
C
T1 N1 T2 N2 T3 N3 T4 N4 T5 N5 T6 N6
MYBL2
GAPDH
T7 N7 T8 N8 T9 N9 T10 N10 T11 N11 T12 N12
MYBL2
GAPDH
D
**
MYBL2 expression score
With distant metastasis
Without distant metastasis
Primary tumor
E
MYBL2
Magnified
Low expression
Negative
Weak
High expression
Moderate
Strong
Case 5
Case 73
Case 63
Case 11
100μm
50μm
F
Metastasis
Tumor thrombus
Tumor size
Percentages
No
Yes
Absent
Present
≥ 11
< 11
ns
High (n=38)
Low (n=40)
G
Overall survival (%)
High MYBL2 (n=38)
Low MYBL2 (n=40)
P=0.046
Time (months)
Progression-free survival (%)
P=0.0415

Figure 6. *MYBL2* functions as an oncogene in HB and predicts metastasis and poor prognosis. A. Expression of *MYBL2* in tumor (n=24) and para-tumor liver (n=24) tissues was analyzed by QPCR assay. B. Expression of MYBL2 in tumor and para-tumor liver tissues was examined by IHC. Scale bars, left: 100 μm; right: 50 μm. C. Comparison of MYBL2 expression in twelve pairs of HB tumors (T) and corresponding normal tissues (N). GAPDH is used as a loading control. D. Expression of MYBL2 in primary HB tumors with metastasis vs HB tumors without metastasis (n=78). E. Representative IHC images of the MYBL2 expression level scored by the SI. Scale bars, left: 100 μm; right: 50 μm. F. Correlation between MYBL2 expression and metastasis, tumor size, and tumor thrombus. G. Kaplan-Meier survival curves show that higher MYBL2 expression is associated with shorter progression-free survival and overall survival.

Table 1. The correlation between the levels of MYBL2 expression and gender, age, tumor thrombus, tumor size, and metastasis in 78 cases of HB tissues by IHC (χ^2 test)

Parameters	MYBL2		*P* values
	High (38 cases)	Low (40 cases)	
Gender			
Male	26	21	0.17
Female	12	19	
Age (months)			
≥17	24	15	0.9999
<17	14	25	
Thrombus			
Present	6	0	0.0089
Absent	32	40	
Size of tumor			
≥11 cm	23	19	0.25
<11 cm	15	21	
Metastasis			
Yes	9	3	0.048
No	29	37	

collectively, these results confirmed the function of MYBL2 in mediating the Smad signaling pathway.

To identify the EMT-inducing transcription factors (TFs), such as SNAI1/2, ZEB1/2, and TWIST1/2 [56], that function as the core factors of the MYBL2-regulated Smad signaling pathway, the mRNA levels of these factors were examined in both MYBL2-upregulated and downregulated cells. Only the levels of *ZEB2* and *SNAI1* were decreased in MYBL2-silenced cells, whereas the levels of *SNAI1/2* and *TWIST2* were increased in MYBL2-overexpressed cells (**Figure 9C**). In addition, increased SNAI1 expression in MYBL2-overexpressed cells was observed by western blotting (**Figure 9D**). These results showed that SNAI1 was a core factor of the MYBL2-mediated Smad signaling pathway.

To investigate the role of the MYBL2-mediated Smad signaling pathway in EMT progression, MYBL2-overexpressing HepG2 cells were cultured in the presence of the Smad pathway inhibitor LY2157299 for 72 h, which was testified by the reduced level of Smad2/3 phosphorylation. Compared with control cells, the EMT course in pathway-inhibited cells was reversed, with an upregulation of the ZO-1 level and a downregulation of the FN1 level, demonstrating that MYBL2 promoted EMT progression by activating the Smad signaling pathway. Furthermore, the level of SNAI1 expression was also decreased by inhibiting the Smad pathway (**Figure 9E**). Taken collectively, these results illustrated that EMT was initiated by the MYBL2-mediated Smad signaling pathway, which was independent of the upregulated SNAI1 expression, and promoted cell migration and HB metastasis.

Discussion

Despite the extremely poor prognosis of lung metastasis in patients with HB, the physiological and pathological mechanisms of metastasis in HB have not been investigated in depth [57, 58]. In this study, we demonstrated the heterogeneity of metastatic cells by scRNA-seq analysis and the oncogenic function and specific mechanism of MYBL2 in HB progression. The application of scRNA-seq enabled us to deconstruct the heterogeneous transcriptional patterns and the exclusive regulatory factors of metastases at the single-cell level. The underlying cellular trajectories predicted by RNA velocity analysis suggested the involvement of EMT in metastasis. Given that EMT progression in vivo is a dynamic and complex process and somewhat difficult to monitor, the role of EMT in promoting tumor metastasis remains controversial. It was reported that knockout of the *Snail1* or *Twist1* gene in a pancreatic ductal adenocarcinoma mouse model did not inhibit tumor invasiveness, tumor spread, and distant metastasis [59]. Incon-

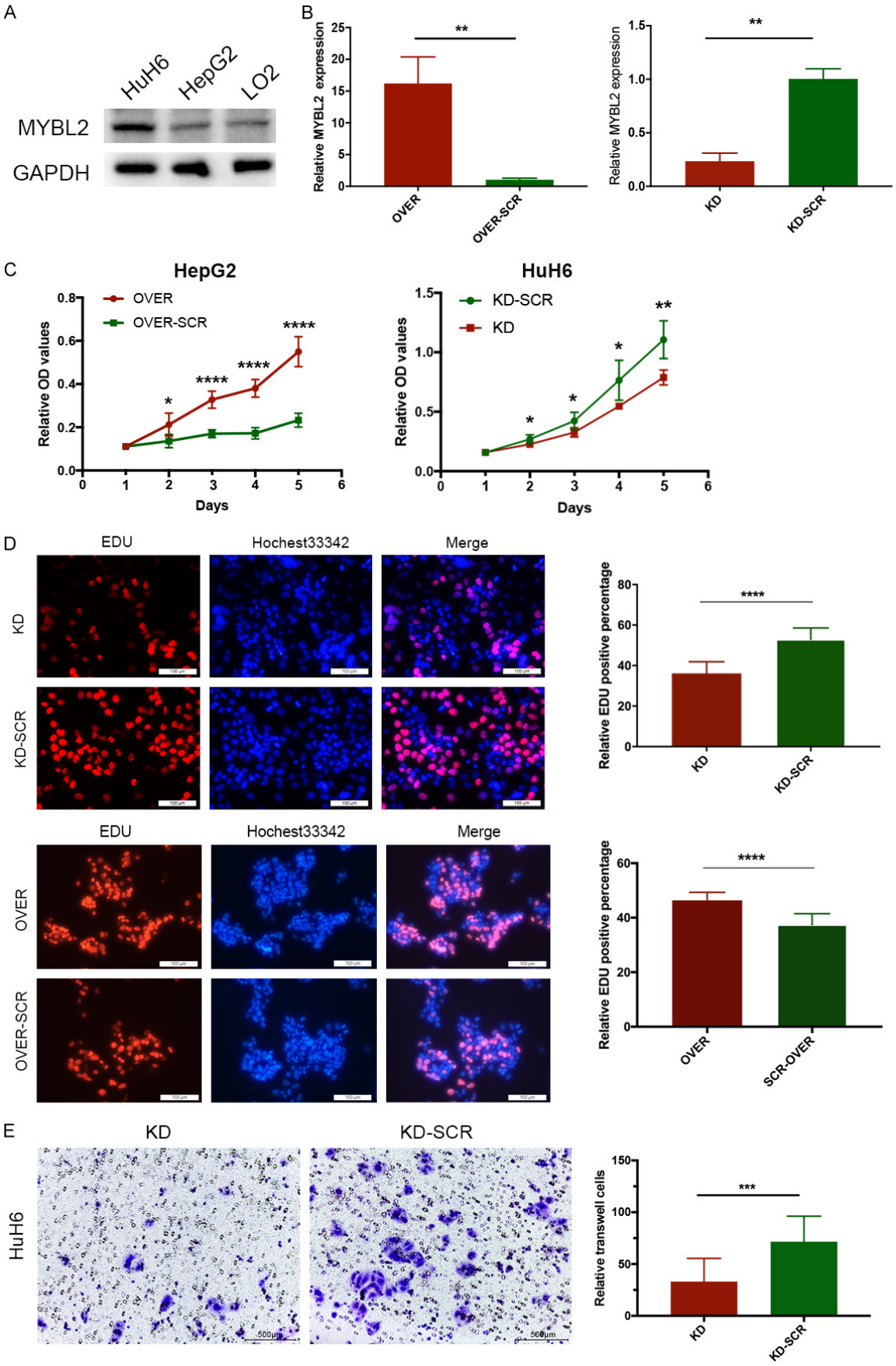
A
HuH6
HepG2
LO2
MYBL2
GAPDH
B
Relative MYBL2 expression
OVER
OVER-SCR
KD
KD-SCR
C
HepG2
HuH6
OVER
OVER-SCR
KD-SCR
KD
Relative OD values
Days
D
EDU
Hochest33342
Merge
KD
KD-SCR
OVER
OVER-SCR
Relative EDU positive percentage
E
KD
KD-SCR
HuH6
Relative transwell cells

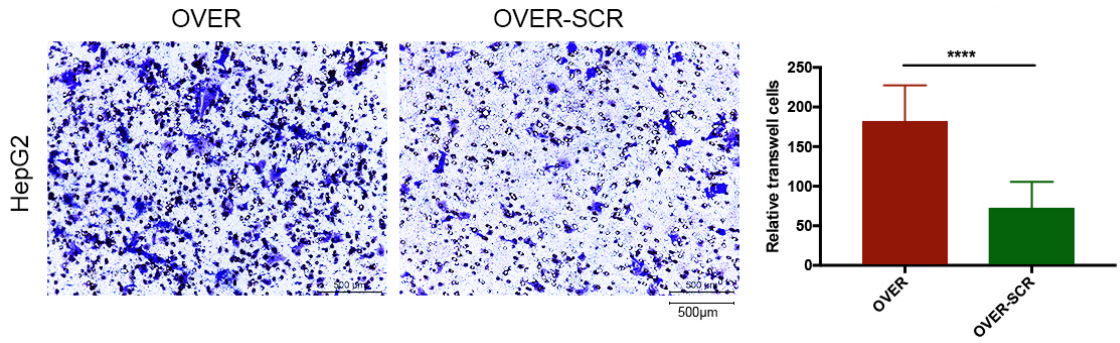

Figure 7. MYBL2 enhances the proliferation and migration of HB cells in vitro. (A) Expression of MYBL2 in two HB cell lines and the normal liver epithelial cell line L02. (B) Ectopic expression of *MYBL2* in *MYBL2*-transfected and sh*MYBL2*-transfected cells was analyzed by QPCR. Results of CCK8 (C) and EdU (D) assays indicate that MYBL2 overexpression enhances the proliferation of HepG2 cells, whereas MYBL2 knockdown inhibits the proliferation of HuH6 cells. Scale bars, 100 μm. (E) Migratory ability of HuH6 and HepG2 cells after modifying MYBL2 expression was examined by the transwell assay. Scale bars, 500 μm.

sistent with the findings of the *Snail1* or *Twist1* gene knockout mouse model, Krebs et al. reported that knockout of the *Zeb1* gene in mice with pancreatic cancer significantly reduced the occurrence of lung metastasis, as well as inhibited stem cell characteristics and tumor-forming ability [54]. As such, the biological processes of EMT may be tissue-specific, and the transcription factors that play key roles in different tumor models may also be variable.

Bioinformatics analysis identified MYBL2 as a potential predictor of metastasis and poor prognosis in patients with HB. Nevertheless, the expression level and biological function of MYBL2 in HB have not been investigated in depth. In this study, we observed that MYBL2 was overexpressed in HB compared with adjacent liver tissues. It also correlated with the occurrence of metastasis and tumor thrombus. Consistent with our findings, enhanced MYBL2 expression was also observed in other malignancies, such as breast, colorectal, and ovarian cancers, and was considered a prognostic marker [60-62]. Furthermore, Bar-shira et al. verified through a public database of prostate cancer that the expression of MYBL2 in metastatic cells was higher than that in primary tumors and benign prostatic hyperplasia [63]. Our study revealed that MYBL2 overexpression stimulated the proliferation and metastatic ability of HB cells, whereas MYBL2 knockdown inhibited the proliferative and metastatic potential of cells using in vitro and in vivo assays. Taken collectively, these results demonstrated the proliferation-promoting and metastasis-promoting roles of MYBL2 in HB.

In this study, we attempted to clarify the relationship and mechanism between MYBL2 and EMT. Our results showed that MYBL2 overexpression promoted EMT and activated the SNAI1-independent Smad signaling pathway, which could be reversed by a Smad signaling pathway inhibitor. SNAI1 was reported to participate in MYBL2-mediated EMT progression in breast cancer [64]. However, the relationship between MYBL2 and the Smad signaling pathway has not been investigated. Jin et al., as well as other researchers, have reported that two heterogeneous subpopulations of mesenchymal-like and epithelial-like tumor cells exist in non-neuroendocrine small cell lung cancer. Compared with the epithelioid subset, the expression of proteins within the TGF-β/Smad signaling pathway was higher in the cell subset with mesenchymal characteristics which had stronger metastatic ability, suggesting the crucial role of TGF-β/Smad-induced EMT in accelerating metastasis and promoting tumor aggressiveness [65].

Taken collectively, the results of this study uncovered the intra-heterogeneity and EMT course of metastatic tissues, as well as identified *MYBL2* as an oncogenic gene that is associated with the metastasis and tumor progression of HB. MYBL2 increased the expression of epithelial markers but decreased the expression of mesenchymal markers. The phosphorylation level of Smad2/3 was upregulat-

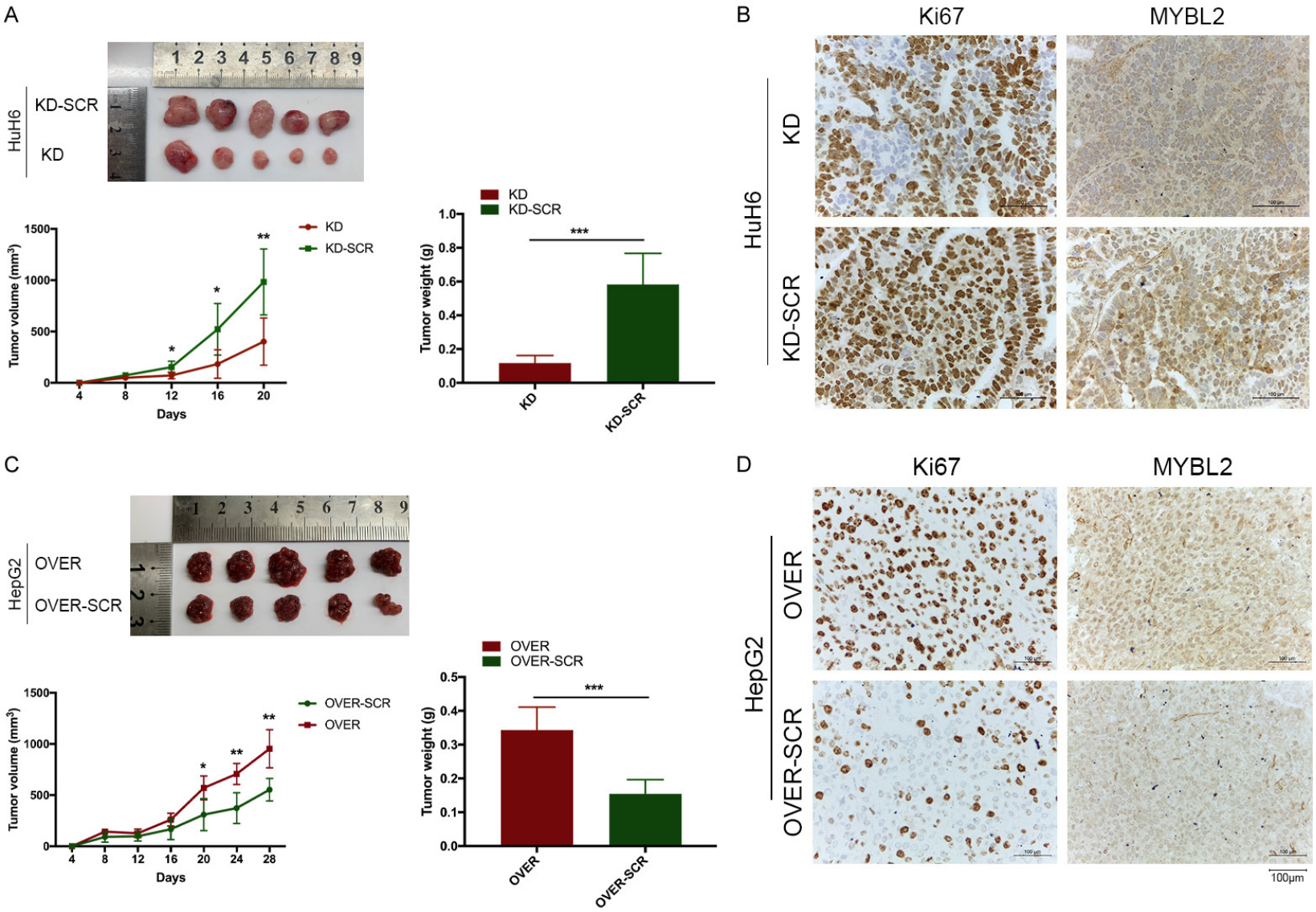

Figure 8. MYBL2 accelerates HB cell proliferation in vivo. A. Top: image of the xenograft tumors formed by MYBL2 downregulation (KD) and control (KD-SCR) HuH6 cells (n=5); bottom-left: growth curve of the xenograft tumors; bottom-right: weight of the xenograft tumors. B. MYBL2 and Ki67 expression in xenograft tumors (KD and KD-SCR) were examined by IHC. Scale bars, 100 μm. C. Top: image of the xenograft tumors formed by MYBL2 upregulation (OVER) and control (OVER-SCR) HepG2 cells (n=5); bottom-left: growth curve of the xenograft tumors; bottom-right: weight of the xenograft tumors. D. MYBL2 and Ki67 expression in xenograft tumors (OVER and OVER-SCR) were examined by IHC. Scale bars, 100 μm.

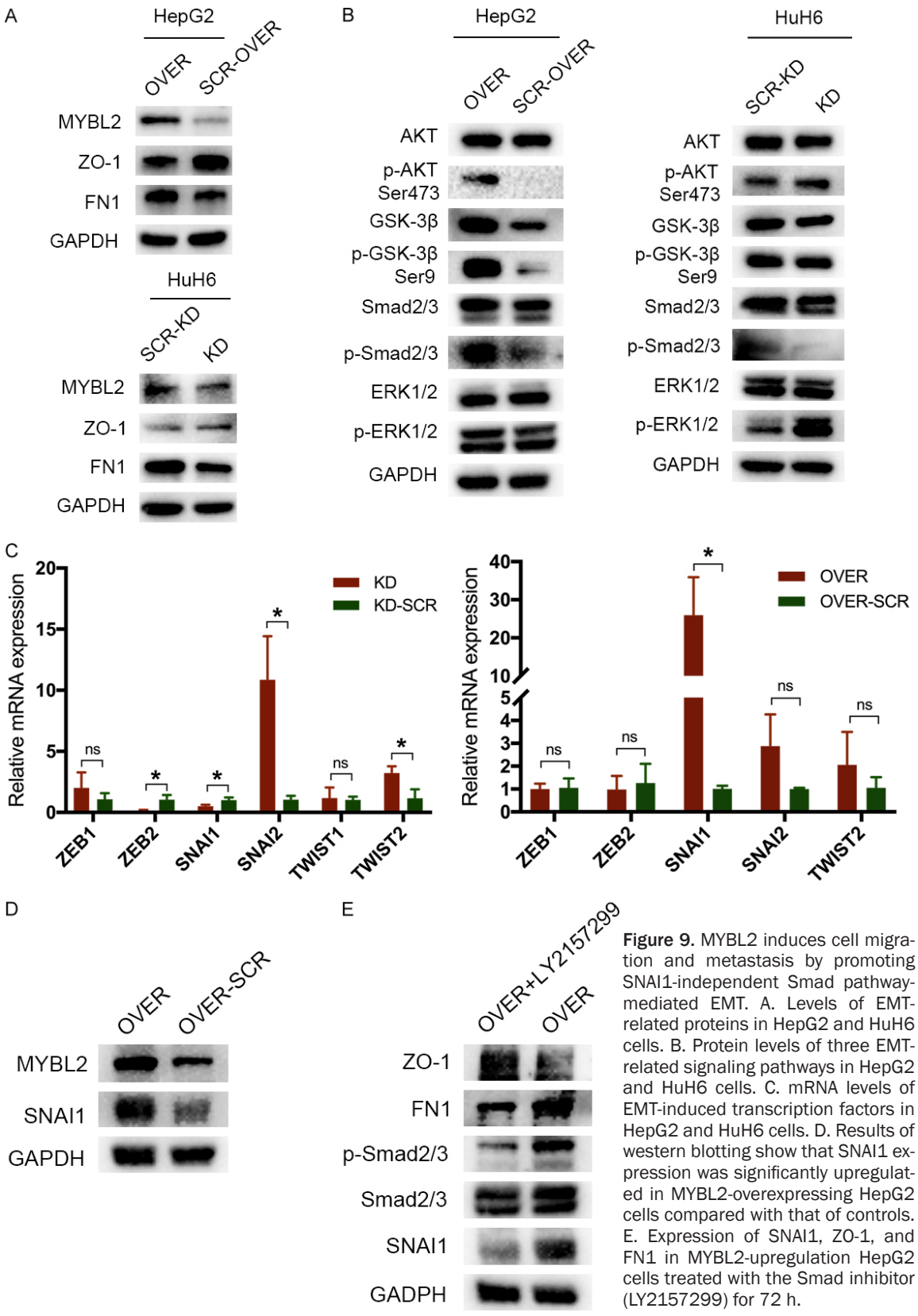

Figure 9. MYBL2 induces cell migration and metastasis by promoting SNAI1-independent Smad pathway-mediated EMT. A. Levels of EMT-related proteins in HepG2 and HuH6 cells. B. Protein levels of three EMT-related signaling pathways in HepG2 and HuH6 cells. C. mRNA levels of EMT-induced transcription factors in HepG2 and HuH6 cells. D. Results of western blotting show that SNAI1 expression was significantly upregulated in MYBL2-overexpressing HepG2 cells compared with that of controls. E. Expression of SNAI1, ZO-1, and FN1 in MYBL2-upregulation HepG2 cells treated with the Smad inhibitor (LY2157299) for 72 h.

ed with MYBL2 overexpression. Furthermore, the MYBL2-induced Smad signaling pathway enhanced the expression of the transcriptional factor SNAI1. Interestingly, enhanced EMT and

the SNAI1-independent Smad signaling pathway can be effectively balanced by inhibiting Smad2/3 phosphorylation. Thus, MYBL2 promoted metastasis of HB by inducing Smad/SNAI1-mediated EMT.

Acknowledgements

This work was supported by the Cyrus Tang Foundation (ZSBK0070), Shanghai Municipal Key Clinical Specialty (no. shslczdzk05703), National Natural Science Foundation of China (no. 82172852), the Shanghai Hospital Development Center (Grant No. SHDC12020125), the Science Foundation of Shanghai (Grant No. 19411966800), and the Children's National Medical Center (Grant No. EK1125180112). The icons and elements in **Figure 1A** were created with BioRender.com. We thank Dr. Jianming Zeng, Xiaoqi Wu, and the bioinformatics team for their reference codes. We thank Lian Wu for preparing the figures using Adobe Illustrator. We thank International Science Editing (http://www.internationalscienceediting.com) for editing this manuscript.

Disclosure of conflict of interest

None.

Address correspondence to: Drs. Kuiran Dong and Rui Dong, Department of Pediatric Surgery, Children's Hospital of Fudan University, 399 Wanyuan Road, Shanghai 201102, China. Tel: +86-18017591156; Fax: +86-21-64931901; E-mail: kuirand@hotmail.com (KRD); Tel: +86-13524415-399; Fax: +86-21-6493190; E-mail: dongrui_1982@126.com (RD)

References

[1] Finegold MJ, Egler RA, Goss JA, Guillerman RP, Karpen SJ, Krishnamurthy R and O'Mahony CA. Liver tumors: pediatric population. Liver Transpl 2008; 14: 1545-56.

[2] Perilongo G, Malogolowkin M and Feusner J. Hepatoblastoma clinical research: lessons learned and future challenges. Pediatr Blood Cancer 2012; 59: 818-821.

[3] Hishiki T, Matsunaga T, Sasaki F, Yano M, Ida K, Horie H, Kondo S, Watanabe K, Oue T, Tajiri T, Kamimatsuse A, Ohnuma N and Hiyama E. Outcome of hepatoblastomas treated using the Japanese Study Group for Pediatric Liver Tumor (JPLT) protocol-2: report from the JPLT. Pediatr Surg Int 2011; 27: 1-8.

[4] Hishiki T, Watanabe K, Ida K, Hoshino K, Iehara T, Aoki Y, Kazama T, Kihira K, Takama Y, Taguchi T, Fujimura J, Honda S, Matsumoto K, Mori M, Yano M, Yokoi A, Tanaka Y, Fuji H, Miyazaki O, Yoshimura K, Takimoto T and Hiyama E. The role of pulmonary metastasectomy for hepatoblastoma in children with metastasis at diagnosis: results from the JPLT-2 study. J Pediatr Surg 2017; 52: 2051-2055.

[5] Yoshida M, Tanaka M, Kitagawa N, Nozawa K, Shinkai M, Goto H and Tanaka Y. Clinicopathological study of surgery for pulmonary metastases of hepatoblastoma with indocyanine green fluorescent imaging. Pediatr Blood Cancer 2021; 10: e29488.

[6] Semeraro M, Branchereau S, Maibach R, Zsiros J, Casanova M, Brock P, Domerg C, Aronson DC, Zimmermann A, Laithier V, Childs M, Roebuck D, Perilongo G, Czauderna P and Brugieres L. Relapses in hepatoblastoma patients: clinical characteristics and outcome - experience of the International Childhood Liver Tumour Strategy Group (SIOPEL). Eur J Cancer 2013; 49: 915-22.

[7] Matsunaga T, Sasaki F, Ohira M, Hashizume K, Hayashi A, Hayashi Y, Mugishima H and Ohnuma N; Japanese Study Group for Pediatric Liver Tumor. Analysis of treatment outcome for children with recurrent or metastatic hepatoblastoma. Pediatr Surg Int 2003; 19: 142-6.

[8] Hu H, Zhang W, Wang Y, Zhang Y, Yi Y, Gao Y, Chen L and Huang D. Prognostic analysis for children with hepatoblastoma with lung metastasis: a single-center analysis of 98 cases. Asia Pac J Clin Oncol 2021; 17: e191-e200.

[9] Nieto MA, Huang RY, Jackson RA and Thiery JP. EMT: 2016. Cell 2016; 166: 21-45.

[10] Yang X and Meng T. MicroRNA-431 affects trophoblast migration and invasion by targeting ZEB1 in preeclampsia. Gene 2019; 683: 225-232.

[11] Owusu-Akyaw A, Krishnamoorthy K, Goldsmith LT and Morelli SS. The role of mesenchymal-epithelial transition in endometrial function. Hum Reprod Update 2019; 25: 114-133.

[12] Kalluri R and Weinberg RA. The basics of epithelial-mesenchymal transition. J Clin Invest 2009; 119: 1420-8.

[13] Ramsay RG and Gonda TJ. MYB function in normal and cancer cells. Nat Rev Cancer 2008; 8: 523-34.

[14] Golay J, Luppi M, Songia S, Palvarini C, Lombardi L, Aiello A, Delia D, Lam K, Crawford DH, Biondi A, Barbui T, Rambaldi A and Introna M. Expression of A-myb, but not c-myb and B-myb, is restricted to Burkitt's lymphoma, sIg+ B-acute lymphoblastic leukemia, and a subset of chronic lymphocytic leukemias. Blood 1996; 87: 1900-11.

[15] Sun SS, Fu Y and Lin JY. Upregulation of MYBL2 independently predicts a poorer prognosis in patients with clear cell renal cell carcinoma. Oncol Lett 2020; 19: 2765-2772.
[16] Hou X, Zhang Y, Han S and Hou B. A novel DNA methylation 10-CpG prognostic signature of disease-free survival reveal that MYBL2 is associated with high risk in prostate cancer. Expert Rev Anticancer Ther 2020; 20: 1107-1119.
[17] Xiong YC, Wang J, Cheng Y, Zhang XY and Ye XQ. Overexpression of MYBL2 promotes proliferation and migration of non-small-cell lung cancer via upregulating NCAPH. Mol Cell Biochem 2020; 468: 185-193.
[18] Jin Y, Zhu H, Cai W, Fan X, Wang Y, Niu Y, Song F and Bu Y. B-Myb is up-regulated and promotes cell growth and motility in non-small cell lung cancer. Int J Mol Sci 2017; 18: 860.
[19] Fan X, Wang Y, Jiang T, Cai W, Jin Y, Niu Y, Zhu H and Bu Y. B-Myb mediates proliferation and migration of non-small-cell lung cancer via suppressing IGFBP3. Int J Mol Sci 2018; 19: 1479.
[20] Guan Z, Cheng W, Huang D and Wei A. High MYBL2 expression and transcription regulatory activity is associated with poor overall survival in patients with hepatocellular carcinoma. Curr Res Transl Med 2018; 66: 27-32.
[21] Jia Y, Gao Y, Li J, Chang Z, Yan J and Qin Y. Prognostic implications of MYBL2 in resected Chinese gastric adenocarcinoma patients. Onco Targets Ther 2019; 12: 1129-1135.
[22] Li Q, Wang M, Hu Y, Zhao E, Li J, Ren L, Wang M, Xu Y, Liang Q, Zhang D, Lai Y, Liu S, Peng X, Zhu C and Ye L. MYBL2 disrupts the Hippo-YAP pathway and confers castration resistance and metastatic potential in prostate cancer. Theranostics 2021; 11: 5794-5812.
[23] Chen X, Lu Y, Yu H, Du K, Zhang Y, Nan Y and Huang Q. Pan-cancer analysis indicates that MYBL2 is associated with the prognosis and immunotherapy of multiple cancers as an oncogene. Cell Cycle 2021; 20: 2291-2308.
[24] Zheng GX, Terry JM, Belgrader P, Ryvkin P, Bent ZW, Wilson R, Ziraldo SB, Wheeler TD, McDermott GP, Zhu J, Gregory MT, Shuga J, Montesclaros L, Underwood JG, Masquelier DA, Nishimura SY, Schnall-Levin M, Wyatt PW, Hindson CM, Bharadwaj R, Wong A, Ness KD, Beppu LW, Deeg HJ, McFarland C, Loeb KR, Valente WJ, Ericson NG, Stevens EA, Radich JP, Mikkelsen TS, Hindson BJ and Bielas JH. Massively parallel digital transcriptional profiling of single cells. Nat Commun 2017; 8: 14049.
[25] Satija R, Farrell JA, Gennert D, Schier AF and Regev A. Spatial reconstruction of single-cell gene expression data. Nat Biotechnol 2015; 33: 495-502.
[26] Butler A, Hoffman P, Smibert P, Papalexi E and Satija R. Integrating single-cell transcriptomic data across different conditions, technologies, and species. Nat Biotechnol 2018; 36: 411-420.
[27] Korsunsky I, Millard N, Fan J, Slowikowski K, Zhang F, Wei K, Baglaenko Y, Brenner M, Loh PR and Raychaudhuri S. Fast, sensitive and accurate integration of single-cell data with Harmony. Nat Methods 2019; 16: 1289-1296.
[28] Tirosh I, Izar B, Prakadan SM, Wadsworth MH 2nd, Treacy D, Trombetta JJ, Rotem A, Rodman C, Lian C, Murphy G, Fallahi-Sichani M, Dutton-Regester K, Lin JR, Cohen O, Shah P, Lu D, Genshaft AS, Hughes TK, Ziegler CG, Kazer SW, Gaillard A, Kolb KE, Villani AC, Johannessen CM, Andreev AY, Van Allen EM, Bertagnolli M, Sorger PK, Sullivan RJ, Flaherty KT, Frederick DT, Jané-Valbuena J, Yoon CH, Rozenblatt-Rosen O, Shalek AK, Regev A and Garraway LA. Dissecting the multicellular ecosystem of metastatic melanoma by single-cell RNA-seq. Science 2016; 352: 189-96.
[29] Venteicher AS, Tirosh I, Hebert C, Yizhak K, Neftel C, Filbin MG, Hovestadt V, Escalante LE, Shaw ML, Rodman C, Gillespie SM, Dionne D, Luo CC, Ravichandran H, Mylvaganam R, Mount C, Onozato ML, Nahed BV, Wakimoto H, Curry WT, Iafrate AJ, Rivera MN, Frosch MP, Golub TR, Brastianos PK, Getz G, Patel AP, Monje M, Cahill DP, Rozenblatt-Rosen O, Louis DN, Bernstein BE, Regev A and Suvà ML. Decoupling genetics, lineages, and microenvironment in IDH-mutant gliomas by single-cell RNA-seq. Science 2017; 355: eaai8478.
[30] Cairo S, Armengol C, De Reyniès A, Wei Y, Thomas E, Renard CA, Goga A, Balakrishnan A, Semeraro M, Gresh L, Pontoglio M, Strick-Marchand H, Levillayer F, Nouet Y, Rickman D, Gauthier F, Branchereau S, Brugières L, Laithier V, Bouvier R, Boman F, Basso G, Michiels JF, Hofman P, Arbez-Gindre F, Jouan H, Rousselet-Chapeau MC, Berrebi D, Marcellin L, Plenat F, Zachar D, Joubert M, Selves J, Pasquier D, Bioulac-Sage P, Grotzer M, Childs M, Fabre M and Buendia MA. Hepatic stem-like phenotype and interplay of Wnt/beta-catenin and Myc signaling in aggressive childhood liver cancer. Cancer Cell 2008; 14: 471-84.
[31] Bergen V, Lange M, Peidli S, Wolf FA and Theis FJ. Generalizing RNA velocity to transient cell states through dynamical modeling. Nat Biotechnol 2020; 38: 1408-1414.
[32] Yin H, Gao T, Xie J, Huang Z, Zhang X, Yang F, Qi W, Yang Z, Zhou T, Gao G and Yang X. FUBP1 promotes colorectal cancer stemness and metastasis via DVL1-mediated activation of Wnt/β-catenin signaling. Mol Oncol 2021; 15: 3490-3512.

[33] Müller S, Liu SJ, Di Lullo E, Malatesta M, Pollen AA, Nowakowski TJ, Kohanbash G, Aghi M, Kriegstein AR, Lim DA and Diaz A. Single-cell sequencing maps gene expression to mutational phylogenies in PDGF- and EGF-driven gliomas. Mol Syst Biol 2016; 12: 889.

[34] Patel AP, Tirosh I, Trombetta JJ, Shalek AK, Gillespie SM, Wakimoto H, Cahill DP, Nahed BV, Curry WT, Martuza RL, Louis DN, Rozenblatt-Rosen O, Suvà ML, Regev A and Bernstein BE. Single-cell RNA-seq highlights intratumoral heterogeneity in primary glioblastoma. Science 2014; 344: 1396-401.

[35] Tomlinson GE, Douglass EC, Pollock BH, Finegold MJ and Schneider NR. Cytogenetic evaluation of a large series of hepatoblastomas: numerical abnormalities with recurring aberrations involving 1q12-q21. Genes Chromosomes Cancer 2005; 44: 177-84.

[36] Yuan J, Levitin HM, Frattini V, Bush EC, Boyett DM, Samanamud J, Ceccarelli M, Dovas A, Zanazzi G, Canoll P, Bruce JN, Lasorella A, Iavarone A and Sims PA. Single-cell transcriptome analysis of lineage diversity in high-grade glioma. Genome Med 2018; 10: 57.

[37] Jessa S, Blanchet-Cohen A, Krug B, Vladoiu M, Coutelier M, Faury D, Poreau B, De Jay N, Hébert S, Monlong J, Farmer WT, Donovan LK, Hu Y, McConechy MK, Cavalli FMG, Mikael LG, Ellezam B, Richer M, Allaire A, Weil AG, Atkinson J, Farmer JP, Dudley RWR, Larouche V, Crevier L, Albrecht S, Filbin MG, Sartelet H, Lutz PE, Nagy C, Turecki G, Costantino S, Dirks PB, Murai KK, Bourque G, Ragoussis J, Garzia L, Taylor MD, Jabado N and Kleinman CL. Stalled developmental programs at the root of pediatric brain tumors. Nat Genet 2019; 51: 1702-1713.

[38] Fong S, Itahana Y, Sumida T, Singh J, Coppe JP, Liu Y, Richards PC, Bennington JL, Lee NM, Debs RJ and Desprez PY. Id-1 as a molecular target in therapy for breast cancer cell invasion and metastasis. Proc Natl Acad Sci U S A 2003; 100: 13543-8.

[39] Aibar S, González-Blas CB, Moerman T, Huynh-Thu VA, Imrichova H, Hulselmans G, Rambow F, Marine JC, Geurts P, Aerts J, van den Oord J, Atak ZK, Wouters J and Aerts S. SCENIC: single-cell regulatory network inference and clustering. Nat Methods 2017; 14: 1083-1086.

[40] Huang JZ, Chen M, Zeng M, Xu SH, Zou FY, Chen D and Yan GR. Down-regulation of TRPS1 stimulates epithelial-mesenchymal transition and metastasis through repression of FOXA1. J Pathol 2016; 239: 186-96.

[41] Su P, Hu J, Zhang H, Jia M, Li W, Jing X and Zhou G. Association of TRPS1 gene with different EMT markers in ERα-positive and ERα-negative breast cancer. Diagn Pathol 2014; 9: 119.

[42] Liu AY, Cai Y, Mao Y, Lin Y, Zheng H, Wu T, Huang Y, Fang X, Lin S, Feng Q, Huang Z, Yang T, Luo Q and Ouyang G. Twist2 promotes self-renewal of liver cancer stem-like cells by regulating CD24. Carcinogenesis 2014; 35: 537-45.

[43] Huang X, Brown C, Ni W, Maynard E, Rigby AC and Oettgen P. Critical role for the Ets transcription factor ELF-1 in the development of tumor angiogenesis. Blood 2006; 107: 3153-60.

[44] Baron VT, Pio R, Jia Z and Mercola D. Early growth response 3 regulates genes of inflammation and directly activates IL6 and IL8 expression in prostate cancer. Br J Cancer 2015; 112: 755-64.

[45] Wouters J, Kalender-Atak Z, Minnoye L, Spanier KI, De Waegeneer M, Bravo González-Blas C, Mauduit D, Davie K, Hulselmans G, Najem A, Dewaele M, Pedri D, Rambow F, Makhzami S, Christiaens V, Ceyssens F, Ghanem G, Marine JC, Poovathingal S and Aerts S. Robust gene expression programs underlie recurrent cell states and phenotype switching in melanoma. Nat Cell Biol 2020; 22: 986-998.

[46] Tsoi J, Robert L, Paraiso K, Galvan C, Sheu KM, Lay J, Wong DJL, Atefi M, Shirazi R, Wang X, Braas D, Grasso CS, Palaskas N, Ribas A and Graeber TG. Multi-stage differentiation defines melanoma subtypes with differential vulnerability to drug-induced iron-dependent oxidative stress. Cancer Cell 2018; 33: 890-904, e5.

[47] Shimba S, Wada T, Hara S and Tezuka M. EPAS1 promotes adipose differentiation in 3T3-L1 cells. J Biol Chem 2004; 279: 40946-53.

[48] Lian M, Chen J, Shen X, Hou L and Fang J. Pparg may promote chemosensitivity of hypopharyngeal squamous cell carcinoma. PPAR Res 2020; 2020: 6452182.

[49] Liu C, Tate T, Batourina E, Truschel ST, Potter S, Adam M, Xiang T, Picard M, Reiley M, Schneider K, Tamargo M, Lu C, Chen X, He J, Kim H and Mendelsohn CL. Pparg promotes differentiation and regulates mitochondrial gene expression in bladder epithelial cells. Nat Commun 2019; 10: 4589.

[50] Nicolai S, Pieraccioli M, Smirnov A, Pitolli C, Anemona L, Mauriello A, Candi E, Annicchiarico-Petruzzelli M, Shi Y, Wang Y, Melino G and Raschellà G. ZNF281/Zfp281 is a target of miR-1 and counteracts muscle differentiation. Mol Oncol 2020; 14: 294-308.

[51] Kim J, Jin H, Zhao JC, Yang YA, Li Y, Yang X, Dong X and Yu J. FOXA1 inhibits prostate cancer neuroendocrine differentiation. Oncogene 2017; 36: 4072-4080.

[52] Wang L and Di LJ. BRCA1 and estrogen/estrogen receptor in breast cancer: where they interact? Int J Biol Sci 2014; 10: 566-75.

[53] Wei T, Weiler SME, Tóth M, Sticht C, Lutz T, Thomann S, De La Torre C, Straub B, Merker S, Ruppert T, Marquardt J, Singer S, Gretz N, Schirmacher P and Breuhahn K. YAP-dependent induction of UHMK1 supports nuclear enrichment of the oncogene MYBL2 and proliferation in liver cancer cells. Oncogene 2019; 38: 5541-5550.

[54] Krebs AM, Mitschke J, Lasierra Losada M, Schmalhofer O, Boerries M, Busch H, Boettcher M, Mougiakakos D, Reichardt W, Bronsert P, Brunton VG, Pilarsky C, Winkler TH, Brabletz S, Stemmler MP and Brabletz T. The EMT-activator Zeb1 is a key factor for cell plasticity and promotes metastasis in pancreatic cancer. Nat Cell Biol 2017; 19: 518-529.

[55] Moustakas A and Heldin CH. Signaling networks guiding epithelial-mesenchymal transitions during embryogenesis and cancer progression. Cancer Sci 2007; 98: 1512-20.

[56] Yamada S, Okumura N, Wei L, Fuchs BC, Fujii T, Sugimoto H, Nomoto S, Takeda S, Tanabe KK and Kodera Y. Epithelial to mesenchymal transition is associated with shorter disease-free survival in hepatocellular carcinoma. Ann Surg Oncol 2014; 21: 3882-90.

[57] Fu X, Cui P, Chen F, Xu J, Gong L, Jiang L, Zhang D and Xiao Y. Thymosin β4 promotes hepatoblastoma metastasis via the induction of epithelial-mesenchymal transition. Mol Med Rep 2015; 12: 127-32.

[58] Zhang Z, Liu F, Yang F and Liu Y. Kockdown of OIP5-AS1 expression inhibits proliferation, metastasis and EMT progress in hepatoblastoma cells through up-regulating miR-186a-5p and down-regulating ZEB1. Biomed Pharmacother 2018; 101: 14-23.

[59] Fischer KR, Durrans A, Lee S, Sheng J, Li F, Wong ST, Choi H, El Rayes T, Ryu S, Troeger J, Schwabe RF, Vahdat LT, Altorki NK, Mittal V and Gao D. Epithelial-to-mesenchymal transition is not required for lung metastasis but contributes to chemoresistance. Nature 2015; 527: 472-6.

[60] Shi H, Bevier M, Johansson R, Grzybowska E, Chen B, Eyfjörd JE, Hamann U, Manjer J, Enquist K, Henriksson R, Carlson J, Brandt A, Lascorz J, Butkiewicz D, Pamula-Pilat J, Tecza K, Herms S, Hoffmann P, Hemminki K, Lenner P and Försti A. Single nucleotide polymorphisms in the 20q13 amplicon genes in relation to breast cancer risk and clinical outcome. Breast Cancer Res Treat 2011; 130: 905-16.

[61] Lassmann S, Weis R, Makowiec F, Roth J, Danciu M, Hopt U and Werner M. Array CGH identifies distinct DNA copy number profiles of oncogenes and tumor suppressor genes in chromosomal- and microsatellite-unstable sporadic colorectal carcinomas. J Mol Med (Berl) 2007; 85: 293-304.

[62] Tanner MM, Grenman S, Koul A, Johannsson O, Meltzer P, Pejovic T, Borg A and Isola JJ. Frequent amplification of chromosomal region 20q12-q13 in ovarian cancer. Clin Cancer Res 2000; 6: 1833-9.

[63] Bar-Shira A, Pinthus JH, Rozovsky U, Goldstein M, Sellers WR, Yaron Y, Eshhar Z and Orr-Urtreger A. Multiple genes in human 20q13 chromosomal region are involved in an advanced prostate cancer xenograft. Cancer Res 2002; 62: 6803-7.

[64] Tao D, Pan Y, Jiang G, Lu H, Zheng S, Lin H and Cao F. B-Myb regulates snail expression to promote epithelial-to-mesenchymal transition and invasion of breast cancer cell. Med Oncol 2015; 32: 412.

[65] Jin Y, Xiao T, Feng Y, Yang J, Guo C, Hu L and Ji H. A mesenchymal-like subpopulation in non-neuroendocrine SCLC contributes to metastasis. J Genet Genomics 2021; 48: 571-581.

Table S1. Sequence of primers

Gene	Forward primer (5'-----3')	Reverse primer (5'-----3')
MYBL2	CACCAGAAACGAGCCTGCCTTA	CTCAGGTCACACCAAGCATCAG
ZEB1	GATGATGAATGCGAGTCAGATGC	ACAGCAGTGTCTTGTTGTTGT
ZEB2	AAAGCTTTCCTGGTCCCATT	GTTGATGGGGCTTGTCATTC
SNAI1	TCGGAAGCCTAACTACAGCGA	AGATGAGCATTGGCAGCGAG
SNAI2	CGAACTGGACACACATACAGTG	CTGAGGATCTCTGGTTGTGGT
TWIST1	AAGAGGTCGTGCCAATCAG	GGCCAGTTTGATCCCAGTAT
TWIST2	AGGCTCTCAGAAGAGGACCC	AAGGAAAAGAATAGCGGCGT
GAPDH	GTCTCCTCTGACTTCAACAGCG	ACCACCCTGTTGCTGTAGCCAA